Manuscript File Click here to view linked References

Wet Etch Methods to Achieve Submicron Active Area Self-Aligned Vertical Sb-heterostructure Backward Diodes

Adam Jönsson[a]*, Pengcheng Xu[a], Julius Reitemeier[b], Paul W. Bohn[b,c], and Patrick Fay[a]

[a]*Electrical Engineering, University of Notre Dame, Notre Dame, United States;*

[b]*Department of Chemistry and Biochemistry, University of Notre Dame, Notre Dame, Indiana 46556, United States*

[c]*Department of Chemical and Biomolecular Engineering, University of Notre Dame, Notre Dame, Indiana 46556, United States*

e-mail: ajonsson@nd.edu, pfay@nd.edu

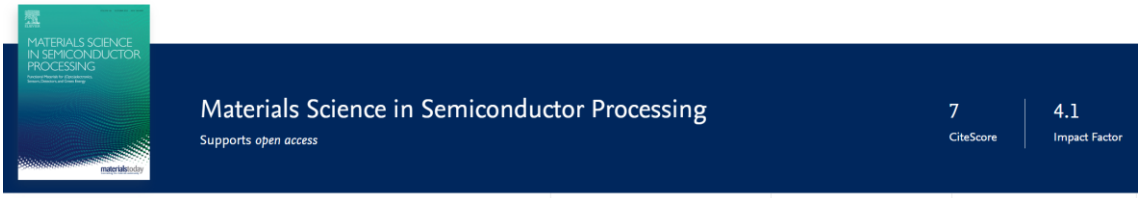

About the journal

Functional Materials for (Opto)electronics, Sensors, Detectors, and Green Energy.

Materials Science in Semiconductor Processing Mrovides a unique forum for the discussion of novel processing, applications, and theoretical studies of functional semiconductor materials and devices. Each issue aims to provide a snapshot of current insights, new achievements, breakthroughs, ...

View full aims & scope

Wet Etch Methods to Achieve Submicron Active Area Self-Aligned Vertical Sb-heterostructure Backward Diodes

We report a citric acid, phosphoric acid, and hydrogen peroxide-based wet etch technique for simplified fabrication of vertical InAs/AlSb/AlGaSb/GaSb heterostructure-based devices. Specifically, we demonstrate this technique in the fabrication of Sb-heterostructure backward diodes with 250 nm height and active diode area down to 0.04 μm^2 (critical dimensions 0.2x0.2 μm^2). The etch chemistry developed here etches the entirety of the heterostructure non-selectively, with little variation in etch rates among the different layers of the heterostructure based on the sequential oxidation of III-V compounds to their respective metal oxides and consecutive dissolution under acidic conditions. Sb-based etch products, including Sb_2O_5, that inhibit etching in conventional citric/peroxide etch chemistries are efficiently removed by the addition of phosphoric acid, facilitating the formation of soluble Sb(V)-citrate complexes. This etch chemistry demonstrates reaction-rate limited behavior and maintains a linear etch rate throughout the InAs/AlSb/AlGaSb/GaSb structure. Reproducibility of the etch method is further verified by current-voltage characterization of diodes with areas varying from 0.04 to 1.8 μm^2.

Keywords: InAs, Sb, heterostructure, diode, detector, MBE

Introduction

Sb-heterostructure (InAs/AlSb/AlGaSb/GaSb) backward diodes are promising devices for direct detection applications in millimeter-wave radiometers due to their superior sensitivity and low noise. [1]–[3] These technologies are especially attractive for passive sensing techniques in, for example, Earth observation instruments (imagers and sounders). [4] For these applications, Sb-heterostructure diodes have demonstrated superior responsivity at high cut-off frequencies with competitive noise equivalent power (0.18 $pW/Hz^{1/2}$), compared to traditional zero-bias Schottky diodes. [5] Employing a molecular-beam epitaxy (MBE) grown Sb-heterostructure also allows tailoring of the layer structure to maximize the application-specific figures of merit.

Furthermore, to achieve the desired noise and performance metrics, defining the active area of the Sb-heterostructure diodes using wet etching is advantageous in order to avoid surface damage caused by dry etch methods. [3], [6] Wet etch methods can also be used to passivate the diode surface to further avoid excess noise sources originating from dangling bonds. [7] A critical issue in sensing in the millimeter-wave and THz regime is down-scaling of the device active area since this allows for improved sensitivity at higher cut-off frequencies. However, due to the undercut that can occur in wet etching, scaling of the device footprint remains a challenge. In this paper, we demonstrate a reduction of 75% in diode active area, to deep submicron dimensions, by utilizing an etchant mixture composed of phosphoric acid, citric acid, and hydrogen peroxide, [8] achieving an area of 0.04 μm^2 as compared to 0.16 μm^2 [3] previously reported in the literature. [9]

The proposed etch and fabrication methods simplify processing and enhance throughput by enabling the use of a continuous single-step etch process for defining the active area of the InAs/AlSb/GaSb heterostructure diode; previous reports required a series of selective etches that are challenging to control. [9] The developed etch method may also be beneficial for fabrication of infrared (IR) detectors for short to long IR wavelength (2 – 30μm) based on InAs/GaSb type II superlattice. [8] The etching conditions are robust and lead to reduced and well-controlled undercut compatible with various metal electrodes allowing for self-aligned diodes with active areas down to 0.04 μm^2, rendering a top-down approach capable of rendering highly scaled Sb-heterostructure diodes by wet-etching, which ultimately improves sensitivity for use in detector application, e.g. mm-wave detectors. [8]

Device Structure

The Sb-heterostructure diodes are based on nearly lattice-matched InAs and Sb-bearing layers grown on top of a GaAs substrate using molecular-beam epitaxy (MBE). A GaAs [100] wafer is used with perpendicular [110] and [1$\bar{1}$0] flats, later referenced during device inspection. The specific heterostructure (from the surface) consists of the following layers: 100 nm n^+InAs, 50 nm n-InAs, 1.5 nm un-intentionally doped (UID) AlSb, 15 nm UID AlGaSb, 50 nm p-GaSb, and 400 nm n^+InAs, on top of semi-insulating GaAs, see Figure 1. The n^+InAs layer serves as the bottom contact in the device, so the active device layers consist of the InAs/AlSb/AlGaSb/GaSb layers above this, corresponding to a thickness of 216.5 nm. The "broken gap" band alignment between InAs and AlGaSb facilitates the nonlinear current-voltage characteristics of the devices, as needed for direct detection applications. [3], [10]

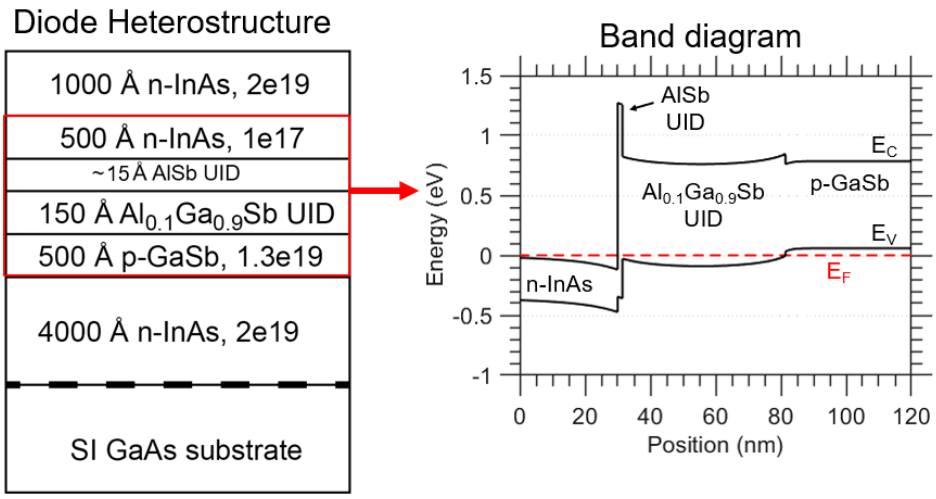

Figure 1: Overview of the designed diode heterostructure highlighting the active layer with the corresponding modeled energy band diagram (1D Poisson solver) at zero bias.

Etch method

Diodes used for direct mm-wave detection require superior sensitivity achieved by both diode non-linearity (current vs. voltage characteristics) as well as device scaling, demanding novel etch techniques to facilitate scaled diode active-region dimensions. Here, this is achieved by wet etching using an aqueous mixture of citric acid, hydrogen peroxide, and phosphoric acid ($C_2H_8O_7$:H_2O_2:H_3PO_4 10 mM:270 mM:680 mM). The etch chemistry is designed to exploit the selective reactivity of each compound in a multi-layered device, such as the Sb-heterostructure described in Figure 1a. Here, we present a detailed description of the sequential multistep etch-mechanism, for all target compounds in the heterostructure, which is based on oxidation of the group 15 partner(s) and subsequent dissolution in acidic conditions.

First, hydrogen peroxide, a strong oxidizing agent with a reduction potential of ~1.76 V vs. normal hydrogen electrode (NHE), [11] reacts with a $M^{(III)}Y^{(-III)}$ metal alloy, where M = In, Ga, Al (group 13 metals) and Y = As, Sb (group 15 metalloids). The reduction potential is well positive of the valence band edge for all of the material compositions, so it lies in the corrosion region. Here, $2e^-/2H^+$ reduction of H_2O_2 (eq. 1) provides the oxidizing equivalents to drive the $8e^-$ oxidation of $Y^{(-III)}$ metalloids to their $Y^{(V)}$-oxides (eq. 2).

$$H_2O_2 + 2H^+ + 2e^- \leftrightharpoons 2H_2O \quad (1)$$

$$2Y^{3-} + 5H_2O \leftrightharpoons Y_2O_5 + 10H^+ + 16\,e^- \quad (2)$$

The overall redox-reaction results in the formation of M_2O_3 and Y_2O_5 metal oxides (eq. 3), so combining the redox ($Y^{(-III)} \rightarrow Y^{(V)}$) and complexation ($MY \rightarrow M_2O_3$) reactions

$$2M^{III}Y^{-III} + 8H_2O_2 \leftrightharpoons M_2O_3 + Y_2O_5 + 8H_2O \quad (3)$$

While the formation of compounds in lower oxidation states, such as Sb, Sb_2O_3, or As_2O_3, is possible, the high concentration of H_2O_2 in combination with low pH (~1.5)

enhance the propensity for reaction (1), suggesting that the fully oxidized species is the dominant reaction product.

After oxidation, the metal oxides undergo dissolution in the highly acidic environment (eq. 4), ultimately etching the material. The presence of phosphoric acid, serves as a source of protons, and it can further aid the etching process by coupling metal oxides that do not readily undergo dissolution in acidic media into their respective phosphates and/or pyrophosphates (eq. 5):

$$M_2O_3 + 6H^+ \leftrightharpoons 2M^{3+} + 6\,H_2O \quad (4)$$

$$M_2O_3 + 2H_3PO_4 \leftrightharpoons 2MPO_4 + 6\,H_2O \quad (5)$$

For example, $GaPO_4$ was found as a by-product when etching GaSb with phosphoric acid. [12] Notably, at a pH ~ 1.5, phosphoric acid predominantly exists in its fully protonated state, H_3PO_4 (pKa ~ 2.1), thus, the impact of dihydrogenphosphate ($H_2PO_4^-$) or more highly deprotonated species (HPO_4^{2-}/PO_4^{3-}) on the etch is marginal.

A major issue arises for the removal of Sb_2O_5, which exhibits low solubility in most acids and bases, and can impede both H_2O_2:H_3PO_4 and H_2O_2:Citric etch solutions. [12], [13] The formation of soluble Sb(V) complexes with multivalent ligands, e.g. tartrate, [13]–[15] is well known and the likely the source of the beneficial etching effect of citric acid is the formation of Sb(V)-citrate complexes in highly acidic environments (eq. 6):

$$Sb(V) + Cit \leftrightharpoons [SbCit] \quad (6)$$

as supported by the observation of Sb(V)-citrate complexes such as $[SbO(CitH_2)_2]$ and $[Sb(OH)_2(CitH_2)_2]$, in mass-spectrometry studies.[13], [16], [17]

Results and discussions

The samples (having the epitaxial structure in Figure 1a) were degreased with N-methyl-2-pyrrolidone (NMP) based solvent at 90 °C, pre-treated with diluted HCl (1:4

DI), followed by lift-off of Ti/Au squares (feature sizes down to 200 nm) defined by electron beam lithography and PMMA/MMA double layer resist. Additional samples with larger patterns were also prepared using Ma-N optical resist as an etch mask for etch rate studies. Citric acid (monohydrate) and phosphoric acid (85 wt%) solution were mixed 24 hours prior to the etch with deionized water to a final concentration of 10 mM and 680 mM, respectively, resulting in pH ~ 1.5. The solution was placed in an ice water bath and stirred using a magnetic stirring rod for 20 minutes to ensure that the citric acid is properly dissolved as well as allowing the solution to reach the target temperature of about 4°C. Hydrogen peroxide (30% aqueous) is added, and the solution is mixed for an additional 5 minutes (resulting volume and weight ratio; $C_2H_8O_7$:H_3PO_4:H_2O_2:H_2O 9g:20ml:12ml:400ml). Adding the hydrogen peroxide in a cooled liquid (4°C) minimizes thermal degradation. [18] Prior to etching the samples, the stir rod is removed, and etching is performed under quiescent conditions. The obtained etching rate against temperature with an Arrhenius plot inset as well as a representative SEM image of the etch result at 4°C and 40°C is presented in Figure 2. The exponential increase in etching rate with increasing temperature indicates that the etch is reaction-rate limited (calculated activation energy of 0.49 eV [19]) rather than diffusion-limited, which is in accordance with a multistep etch mechanism including a rate-limiting step. Performing the etch at reduced temperatures, with slower kinetics, serve to significantly reduce the lateral undercut (see Figure 2b, compare 4^{o}C and 40^{o}C), by promoting the formation of higher density (slower etching) crystal planes that aid in achieving anisotropy. [20]

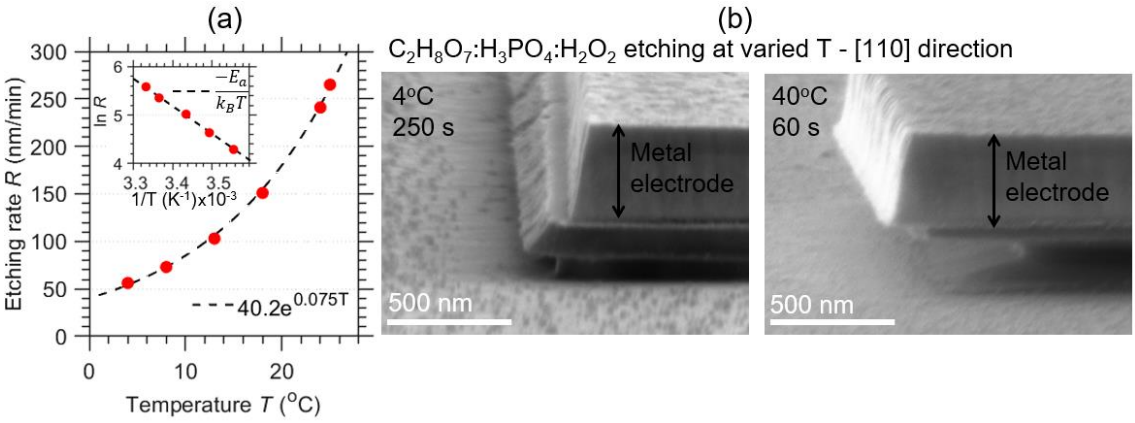

Figure 2: (a) Measured Etching rate R vs Temperature T (°C) following the expected trend for a reaction-rate limited etch regime, inset illustrates calculation of activation energy E_a=0.49 eV from an Arrhenius plot (ln R vs $1/T$ (K^{-1}), Boltzmann constant k_B). [19] (b) Oblique SEM imaging of wet etching results at 4°C and 40°C respectively using Ti/Au (30/300 nm) metal electrode as an etch mask highlighting the decreased mask undercut with lower temperature.

Figure 3 presents the measured etch depth vs time of the proposed etch solution ($C_2H_8O_7$:H_3PO_4:H_2O_2) at 4°C and 21°C (room temperature) respectively as well as oblique SEM images of etched heterostructure at varied time. To explore the role of citric acid within the mixture, additional etching experiments were conducted in the absence of citric acid (H_3PO_4:H_2O_2) at 4°C (Figure 3a). In the absence of citric acid, the resulting etching rate of the InAs layer is slightly increased, rising from 54 nm/min to 59 nm/min. However, the phosphoric-only etchant slows significantly when reaching the Sb-containing layer, after which the etching rate behaves non-linearly. In contrast, in the presence of citric acid, the etch rate is constant throughout the Sb-containing layer, consistent with the formation of soluble Sb(V)-citrate complexes [13], [16], [17] in highly acidic conditions as discussed above (see Etch method section). The etch rates of both etching solutions at 4°C are summarized in Table 1.

The oblique-incidence SEM images of etch results at 140 s, 240 s and 280 s (for separate samples) using a Ti/Au etch mask (square 0.5x0.5 μm^2) are presented in Figure 3b. Different crystal faces for the different material compositions within the heterostructure are clearly visible.

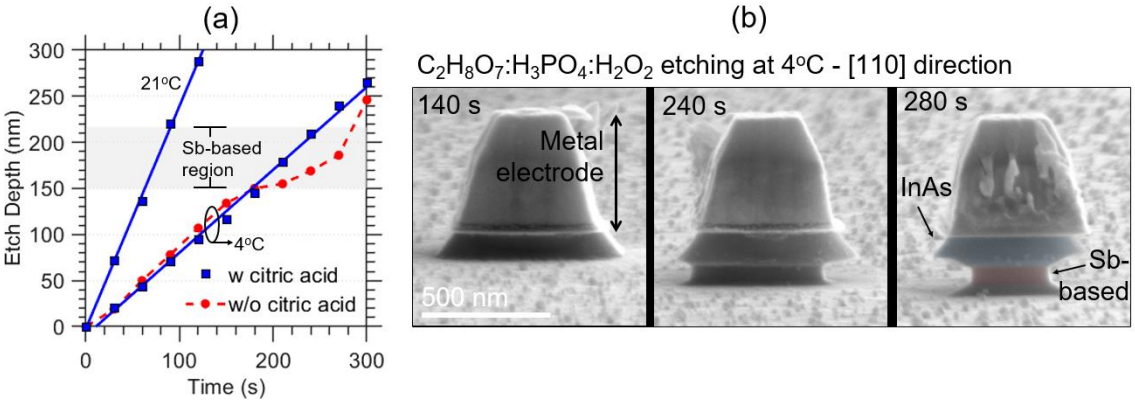

Figure 3: (a) Etch depth vs time using the $C_2H_8O_7$:H_3PO_4:H_2O_2 mixture (10 mM:270 mM:680 mM) at 4°C and 21°C (room temperature) and a H_3PO_4:H_2O_2 mixture (270 mM:680 mM) in the absence of citric acid at 4°C. (b) Oblique SEM inspection of an etched structure using citric and orthophosphoric etch solution with a square 0.5x0.5 μm^2 metal (Ti/Au) electrode etch mask for 140, 240 and 280 s etch time (separate samples).

Table 1: Etching rate of InAs and Sb-based layers (AlSb/AlGaSb/GaSb) at temperature T = 4°C for different combinations citric acid, orthophosphoric acid and hydrogen peroxide.

Solution at T=4°C	Etching rate InAs	Etching rate Sb-based layers
$C_2H_8O_7$:H_3PO_4 10 mM:270 mM	<1 nm/min	<1 nm/min
H_3PO_4:H_2O_2 270 mM:680 mM	59 nm/min	~30 nm/min
$C_2H_8O_7$:H_3PO_4:H_2O_2 10 mM:270 mM:680 mM	54 nm/min	54 nm/min

As noted above, despite the advantages of dry etching for the formation of nanoscale, high-aspect ratio features, wet etching is advantageous for the fabrication of these devices to avoid sidewall damage that can arise in dry etch processing. To confirm the integrity of the sidewalls in the fabricated structures, the electrical current-voltage (IV) characteristics of diodes fabricated using the proposed etch were recorded. In addition, the DC performance metrics junction resistance and curvature for 190 diodes on the same chip were extracted from the measured current-voltage characteristics and are shown in Figure 4. Here, curvature γ quantifies the non-linearity (responsivity) of the diode at zero bias defined as $\frac{\partial^2 I}{\partial V^2} / \frac{\partial I}{\partial V}$ and junction resistance is calculated as the inverse slope $\frac{\partial V}{\partial I}$ at zero bias. In the absence of sidewall damage, the current should scale with respect to diode area, varying from 0.04-1.80 μm^2, and the junction resistance should scale inversely with area. As shown in Fig. 4(a), (b), this expected trend is observed; the junction resistance scaling closely following the 1/area trend (Figure 4b) indicates the absence of sidewall depletion or damage effects. The diodes also show consistent zero-bias curvature, independent of area as expected. Due to the well-controlled non-selective and reaction-rate limited etching, excellent yield is achieved with reproducible undercut and etch depth, resulting in limited variation of performance metric statistics over 190 devices on the same chip.

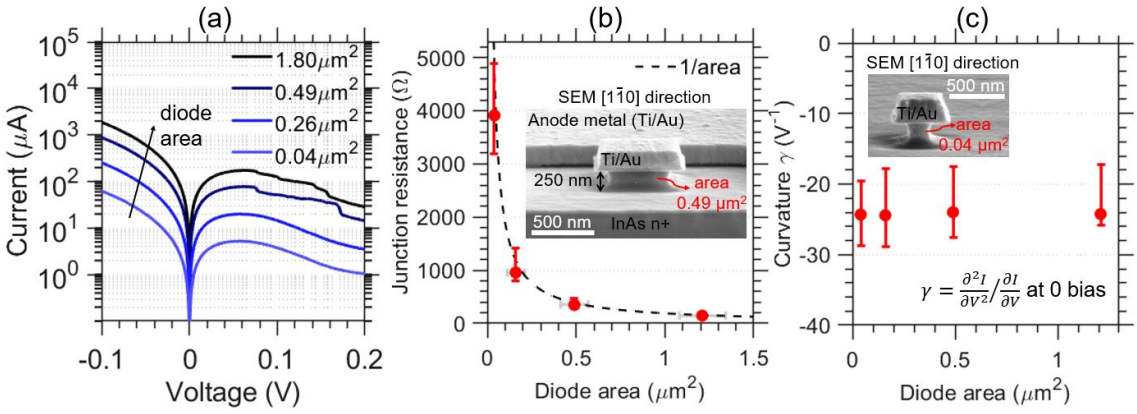

Figure 4: Overview of the electrical performance of the fabricated diodes. (a) Representative current vs voltage characteristics for effective diode areas (determined by oblique SEM inspections) of 1.80, 0.49, 0.26 and 0.04 μm^2, respectively. (b)-(c) Statistics of performance metrics (at zero bias) for 190 devices with varied cross-sectional device area on the same chip, with insets of an oblique SEM image of representative etched diode structure with Ti/Au (30/200 nm) anode and cathode contact and 0.49 μm^2 active area. (b) Junction resistance vs diode cathode area with device area variation. Dashed line represents the expected area vs resistance scaling (1/area). (c) Curvature vs diode area, showing a slight decline in curvature for larger devices with an inset of an oblique SEM image of a representative 0.04 μm^2 area diode.

Conclusion

Vertical Sb-heterostructure backward diodes with active area down to 0.04 μm^2 have been fabricated using a citric acid-phosphoric acid-hydrogen peroxide wet etch composition. Here, using wet etching, as compared to dry etching, is a prerequisite for limiting induced surface damage. The developed wet etch method achieves high throughput and excellent reproducibility by non-selective etching of InAs/AlSb/AlGaSb/GaSb heterostructure by exploiting a combination of chemical oxidation, acidic dissolution, and complexation. The crucial role of interaction between phosphoric and citric acids to obtain a homogenous etch through Sb-containing layers was demonstrated, suggesting the formation of soluble Sb(V)-citrate complexes under acidic conditions facilitates removal of Sb_2O_5 etch products. It was also found that performing the etch at lower temperatures (4°C), is imperative to reduce lateral mask undercut, ultimately enabling deep sub-micron device footprints. Thus, we have achieved well-controlled and anisotropic wet etching of an InAs/Sb-bearing heterostructures, used to realize diodes with active areas as small as 0.04 μm^2 that

facilitates next-generation Earth observation instruments by enhanced millimeter-wave direct detection. Statistics of diode performance metrics derived from current-voltage characterization further solidifies the reproducibility of the proposed etch method.

Acknowledgements

This work was supported by 3rd NASA Earth Venture Mission (EVM-3), specifically INvestigation of Convective UpdraftS (INCUS). The project was also partly supported by National Science Foundation grant 2303574. The author extends his gratitude to Pekka Kangaslahti and Maryam Salim at Jet Propulsion Laboratory (JPL) for valuable input.

References

[1] P. Piironen, "Millimetre-Wave Direct Detection Receivers for Earth Observation Instruments - Trends and Challenges," *GSMM 2022 - 14th Global Symposium on Millimeter-Waves and Terahertz*, pp. 74–77, 2022, doi: 10.1109/GSMM53818.2022.9792364.

[2] D. Petkie, F. De Lucia, C. Castro, P. Helminger, E. Jacobs, al T. Douglas Petkie, F. C. De Lucia, E. L. Jacobs, S. K. Moyer, S. Murrill, C. Halford, S. Griffin, D. T. Petkie, C. Casto, and C. Franck, "Active and passive millimeter- and sub-millimeter-wave imaging," *https://doi.org/10.1117/12.638982*, vol. 5989, no. 7, pp. 359–366, Nov. 2005, doi: 10.1117/12.638982.

[3] Z. Zhang, R. Rajavel, P. Deelman, and P. Fay, "Sub-micron area heterojunction backward diode millimeter-wave detectors with 0.18 pW/Hz1/2 noise equivalent power," *IEEE Microwave and Wireless Components Letters*, vol. 21, no. 5, pp. 267–269, May 2011, doi: 10.1109/LMWC.2011.2123878.

[4] S. Padmanabhan, T. C. Gaier, A. B. Tanner, S. T. Brown, B. H. Lim, S. C. Reising, R. Stachnik, R. Bendig, and R. Cofield, "TEMPEST-D Radiometer: Instrument Description and Prelaunch Calibration," *IEEE Transactions on Geoscience and Remote Sensing*, vol. 59, no. 12, pp. 10213–10226, Dec. 2021, doi: 10.1109/TGRS.2020.3041455.

[5] Z. Zhang, R. Rajavel, P. Deelman, and P. Fay, "Sub-micron area heterojunction backward diode millimeter-wave detectors with 0.18 pW/Hz1/2 noise equivalent power," *IEEE Microwave and Wireless Components Letters*, vol. 21, no. 5, pp. 267–269, May 2011, doi: 10.1109/LMWC.2011.2123878.

[6] S. Murad, M. Rahman, N. Johnson, S. Thoms, S. P. Beaumont, and C. D. W. Wilkinson, "Dry etching damage in III–V semiconductors," *Journal of Vacuum Science & Technology B: Microelectronics and Nanometer Structures Processing, Measurement, and Phenomena*, vol. 14, no. 6, pp. 3658–3662, Nov. 1996, doi: 10.1116/1.588745.

[7] R. Chaghi, C. Cervera, H. Aït-Kaci, P. Grech, J. B. Rodriguez, and P. Christol, "Wet etching and chemical polishing of InAs/GaSb superlattice photodiodes," *Semicond Sci Technol*, vol. 24, no. 6, p. 065010, May 2009, doi: 10.1088/0268-1242/24/6/065010.

[8] A. Kowalewski, P. Martyniuk, O. Markowska, D. Benyahia, and W. Gawron, "New wet etching solution molar ratio for processing T2SLs InAs/GaSb nBn MWIR infrared detectors grown on GaSb substrates," *Mater Sci Semicond Process*, vol. 41, pp. 261–264, Jan. 2016, doi: 10.1016/J.MSSP.2015.08.034.

[9] N. Su, Y. Tang, Z. Zhang, T. F. Kuech, and P. Fay, "Observation and control of electrochemical etching effects in the fabrication of InAs⁄AlSb⁄GaSb heterostructure devices," *Journal of Vacuum Science & Technology B:*

Microelectronics and Nanometer Structures, vol. 26, no. 3, p. 1025, 2008, doi: 10.1116/1.2924328.

[10] J. N. Schulman and D. H. Chow, "Sb-heterostructure interband backward diodes," *IEEE Electron Device Letters*, vol. 21, no. 7, pp. 353–355, Jul. 2000, doi: 10.1109/55.847378.

[11] A. J. Bard and L. R. Faulkner, "Electrochemical methods : fundamentals and applications," p. 833, Accessed: Aug. 14, 2023. [Online]. Available: https://www.wiley.com/en-us/Electrochemical+Methods%3A+Fundamentals+and+Applications%2C+2nd+Edition-p-9781118312803

[12] V. A. Karavanskii, V. N. Denisov, and B. N. Mavrin, "Identifying the by-products on the surface of porous GaAs and GaSb semiconductors by Raman scattering," *Journal of Optical Technology, Vol. 69, Issue 2, pp. 67-*, vol. 69, no. 2, pp. 67-, Feb. 2002, doi: 10.1364/JOT.69.000067.

[13] J. Zheng, A. Iijima, and N. Furuta, "Complexation effect of antimony compounds with citric acid and its application to the speciation of antimony(III) and antimony(V) using HPLC-ICP-MS," *J Anal At Spectrom*, vol. 16, no. 8, pp. 812–818, Jan. 2001, doi: 10.1039/B101943K.

[14] O. Dier, L. Lin Chun, M. Grau, and M. C. Amann, "Selective and non-selective wet-chemical etchants for GaSb-based materials," *Semicond Sci Technol*, vol. 19, no. 11, pp. 1250–1253, Nov. 2004, doi: 10.1088/0268-1242/19/11/006.

[15] J. G. Buglass, T. D. McLean, and D. G. Parker, "A Controllable Etchant for Fabrication of GaSb Devices," *J Electrochem Soc*, vol. 133, no. 12, pp. 2565–2567, Dec. 1986, doi: 10.1149/1.2108472/XML.

[16] H. R. Hansen and S. A. Pergantis, “Investigating the formation of an Sb(V)–citrate complex by HPLC-ICP-MS and HPLC-ES-MS(/MS),” *J Anal At Spectrom*, vol. 21, no. 11, pp. 1240–1248, Oct. 2006, doi: 10.1039/B607621A.

[17] H. R. Hansen and S. A. Pergantis, “Detection of antimony species in citrus juices and drinking water stored in PET containers,” *J Anal At Spectrom*, vol. 21, no. 8, pp. 731–733, Jul. 2006, doi: 10.1039/B606367E/.

[18] Z. Hong, K. Y. Lam, R. Sur, S. Wang, D. F. Davidson, and R. K. Hanson, “On the rate constants of OH + HO2 and HO2 + HO2: A comprehensive study of H2O2 thermal decomposition using multi-species laser absorption,” *Proceedings of the Combustion Institute*, vol. 34, no. 1, pp. 565–571, Jan. 2013, doi: 10.1016/J.PROCI.2012.06.108.

[19] H. D. Um, N. Kim, K. Lee, I. Hwang, J. Hoon Seo, Y. J. Yu, P. Duane, M. Wober, and K. Seo, “Versatile control of metal-assisted chemical etching for vertical silicon microwire arrays and their photovoltaic applications,” *Scientific Reports 2015 5:1*, vol. 5, no. 1, pp. 1–11, Jun. 2015, doi: 10.1038/srep11277.

[20] M. J. Cich, J. A. Johnson, G. M. Peake, and O. B. Spahn, “Crystallographic dependence of the lateral undercut wet etching rate of InGaP in HCl,” *Appl Phys Lett*, vol. 82, no. 4, pp. 651–653, Jan. 2003, doi: 10.1063/1.1540236.

Declaration of interests

☐The authors declare that they have no known competing financial interests or personal relationships that could have appeared to influence the work reported in this paper.

☒The authors declare the following financial interests/personal relationships which may be considered as potential competing interests:

Adam Jonsson reports financial support was provided by Jet Propulsion Laboratory. Pengcheng Xu reports financial support was provided by Jet Propulsion Laboratory. Patrick Fay reports financial support was provided by Jet Propulsion Laboratory. Julius Reitemeier reports financial support was provided by National Science Foundation. Paul W. Bohn reports financial support was provided by National Science Foundation.

Authors' contribution

Dr. Adam Jönsson developed and optimized the device processing including various etch chemistries, performed electrical measurements, and designed the study and wrote the manuscript draft. Pengcheng Xu performed further device optimization and electrical characterization leading to the electrical data presented within the study. Julius Reitemeier outlined the detailed theoretical formalism behind the etch chemistry together with an extensive literature study and provided guidance for the direction of the study, thus was a part of the writing process. Prof. Paul W. Bohn provided funding for the chemistry and provided extensive input on the analysis. Prof. Patrick Fay supervised, coordinated, designed the underlying project including funding, provided material, technical assistance, and provided extensive input with respect to the paper content. All authors read and approved the manuscript.

Dr. Adam Jonsson (conception and design, conducting experiments, manuscript writing, data analysis, interpretation of data, collecting data)

Pengcheng Xu (conducting experiment, interpretation of data, collecting data)

Julius Reitemeier (manuscript writing, data analysis, interpretation of data, conception and design)

Professor Paul W. Bohn (manuscript writing, obtaining funding, interpretation of data)

Professor Patrick Fay (manuscript writing, data analysis, interpretation of data, obtaining funding, project management, providing samples, technical assistance)